Technical Physics, 2024, Vol. 69, No. 11

05

Experimental Study of Strain Hardening in Cast Austenitic 60X24AG16 Steel

© E.E. Deryugin, I.V. Vlasov, Yu.F. Gomorova

Institute of Strength Physics and Materials Science, Siberian Branch, Russian Academy of Sciences,
634055 Tomsk, Russia
e-mail: gomjf@ispms.ru

Received June 4, 2024
Revised August 4, 2024
Accepted August 19, 2024

An improved method for the numerical determination of the deformation characteristics of low-ductility materials is presented. A specialized algorithm has been developed that, using the capabilities of the standard OriginPro software, enables accurate averaging of the experimental deformation diagram and represents it in an analytical form. The nonlinear part of the experimental stress-strain relationship is expressed as a 9th-degree polynomial. This analytical representation of the deformation diagram allowed for a precise determination dependency of the strain hardening coefficient and the strain hardening rate of the material from deformation. Using this new method, the patterns of strain hardening in the cast 60X24AG16 alloy were analyzed. Special attention is given to the influence of preliminary deformation on the strain hardening characteristics.

Keywords: uniaxial tension, three-point bending, strain hardening, preloading, deformation stages, boundary conditions, numerical analysis of tensile curves.

DOI: 10.61011/TP.2024.11.59746.199-24

Introduction

TRIP (transformation induced plasticity) steels are new generation materials which are distinguished not only by high mechanical properties, but also by excellent plasticity in a fairly wide range from 5 to 30% [1–5]. The abbreviation TRIP means transformation induced plasticity [4]. TRIP steels have a multiphase structure containing ferrite, bainite and residual austenite, which is obtained as a result of a two-stage heat treatment process by holding the steel in a two-phase austenitic-ferritic range and followed by exposure in the bainite transformation range. TRIP steels with a high content of residual austenite have the best mechanical properties. For example, TRIP steels with a high manganese (Mn) content have high ductility (up to $\varepsilon_p = 19\%$) and high strength (> 700 MPa) [5]. Thermomechanical treatment of TRIP steels is an expensive operation.

On the other hand, both the temperature and the annealing time are always limited on industrial lines [6]. This means that the equilibrium fractions of the phases and the equilibrium content of the substitutive solutes in the various phases are never reached. Especially, this also applies to cast steels. Consequently, residual austenite remains in the volume of the sample and the TRIP effect is manifested to a certain extent and plasticity is present. In particular, a similar mechanism of plastic strain was found in the cast austenitic alloy 60X24AG16 [7], containing an increased content of carbon (0.57%) and nitrogen (0.70%). As a rule, cast alloys are low-plastic. Nevertheless, cast low-plastic alloys can be widely used if, with low plasticity, they have high strength properties on a par with high-strength steels. Therefore, the study of strain hardening of low-plastic alloys is important for engineering applications.

The paper [8] describes an original method for numerically determination of the characteristics of strain hardening of a material based on experimental strain diagrams of cast steel 60X24AG16 using the capabilities of the standard OriginPro program. The coefficient of strain hardening θ was determined by the ratio of the difference of the applied force ΔP to the difference of strain $\Delta\lambda$ between two points on the strain diagram spaced at a certain distance from each other: $\theta = \Delta P/\Delta\lambda$. It was shown that the spread of points on curves $\theta - \lambda$ decreases with the increase of the distance between points. However, the transition from $P - \lambda$ to $\theta - \lambda$ is accompanied by a significant reduction in the strain interval, within which the dependence $\theta - \lambda$ is determined. This makes it difficult to obtain accurate values of θ and correctly compare the values of P and θ corresponding to the same degree of strain. For this reason a further improvement of existing methods for determining the dependence of the characteristics of strain hardening of a material on the degree of strain is an urgent problem of strength physics, especially for low-plastic materials.

The purpose of this paper is to present an improved method for numerical analysis of the strain characteristics of low-plastic materials and, based on it, to analyze the patterns of strain hardening of cast alloy 60X24AG16 according to experimental strain diagrams.

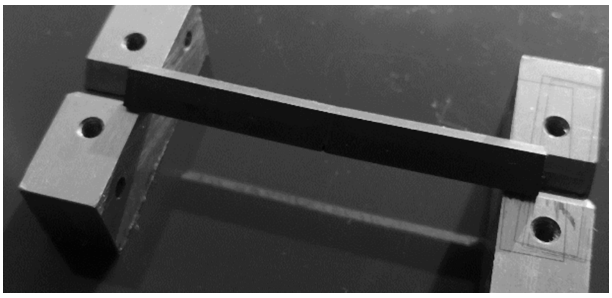

Figure 1. Sample is placed with edge on the supports.

1. Experimental procedure

The material of the study is cast austenitic nitrogenous steel 60X24AG16 of the following chemical composition (% by weight): 24.40 Cr; 16.40 Mn; 1.10 Si; 0.18 Ni; 0.57 C; 0.70 N; 0.017 S; the rest is Fe.

Rods with a square cross section 5×5 mm and a length of 50 mm were tested using the three-point deflection method. The samples were placed on the supports with an edge, as shown in Fig. 1. Such an unconventional arrangement of samples on supports was used to prolong the stage of inelastic strain and steady crack propagation [7]. The supports were located at a distance of 48 mm from each other.

Flat samples with stretching heads were cut from the ingot using the electroerosion method. The cross section of the sample and the length of the working part were 5×5 mm and 48 mm, respectively.

The samples were loaded using the Instron 5582 testing machine (Instron, USA) with a vertical traverse velocity of 0.3 mm/min. At least three samples were tested for each specific strain mode. Eventually, a digital record of the strain diagram of the material under the specified boundary conditions of strain was obtained.

A special algorithm was developed for determining the mechanical characteristics of the material that allows determining the dependence of the coefficient of strain hardening θ on the magnitude of strain λ with great accuracy according to experimental strain diagrams. In addition, the dependence of the rate of decrease of the strain hardening coefficient $\eta = \Delta\theta/\Delta\lambda$ on strain was determined using a similar algorithm based on the obtained dependence $\theta - \lambda$. The resulting diagrams recorded in coordinates „force P-traverse displacement λ" were analyzed numerically using an algorithm developed for this purpose using the capabilities of the standard OrigionPro program.

2. Numerical analysis of experimental loading diagrams

Hypothetically, the strain diagram is represented as a smooth dependence curve „$P - \lambda$", where P force or stress, and λ displacement or strain. The nature of the accumulation of inelastic strain in the sample volume is judged primarily by the change of the strain hardening coefficient (SHC) $\theta = dP/d\lambda$. Additional information can be obtained by determining the change in the coefficient θ from strain λ, namely $\eta = d\theta/d\lambda$. In other words, the hardening of the material can be judged if the dependence of the first and second order derivatives $\theta = dP/d\lambda$ and $\eta = dP/d\lambda = d^2P/d\lambda^2$ on the parameter λ is known. In fact, the experimental diagram „$P - \lambda$" is discrete and consists of a digital record of points in coordinates „$P - \lambda$". The coefficient θ in this case, with a certain accuracy, is found as the ratio of the difference of the applied force ΔP to the difference of deflection $\Delta\lambda$ between points at a certain distance from each other $\theta = \Delta P/\Delta\lambda$. This approach was used in Ref. [8]. It was shown that the greater the distance between the points, the smaller the spread of points on the dependence curve $\theta - \lambda$. However, the numerical values of θ deviate more and more from the theoretical ones. In addition, each transition from $P - \lambda$ to $\theta - \lambda$ and further from $\theta - \lambda$ to $\eta - \lambda$ is accompanied by a significant reduction of the strain interval within which these dependencies are determined. For this reason, any correct comparison and accuracy of the values P, θ and λ corresponding to the same degree of strain is complicated.

A special algorithm was developed to avoid these disadvantages that allows for a correct averaging of strain diagram using the capabilities of the standard OriginPro program and presenting it in an analytical form. The experimental dependence $P - \lambda$ was divided into two parts, elastic and nonlinear, for this purpose. The dependence $P - \theta$ is linear at the elastic strain stage and can be written as $P = \theta_{\max}\lambda$. The first derivative at this stage is $dP/d\lambda = \text{const} = \theta_{\max}$ by definition.

The nonlinear part of the dependence $P - \lambda$ was represented analytically as a polynomial of the 9th degree, using the capabilities of the standard OriginPro program. The analytical representation of the dependence $P - \lambda$ allowed using the approach proposed in Ref. [8], using the minimum and constant distance $d\lambda$ between neighboring points of the polynomial record. Obviously, the derivative $\theta = dP/d\lambda$ is determined with optimal accuracy at each point of dependence $P - \lambda$, and the derivative $d\theta/d\lambda$, or the second derivative $d^2P/d\lambda^2$ are determined in dependence $\theta - \lambda$.

In the general case, the SHC is a nonlinear strain function. The SHC is maximal $\theta = \theta_{\max}$ at the linear stage of strain. $\theta = dP/d\lambda$ cannot exceed $\theta_{\max}$ in the entire strain interval. As a rule, *theta* decreases in the process of plastic strain. The change of the coefficient of strain hardening $d\theta/d\lambda = \eta$ during strain in the scientific literature is commonly referred to as the rate of strain hardening or the rate of hardening [9,10]. The dependence $\eta - \lambda$ provides additional information about the mechanisms of plastic strain in the volume of the material. $d\theta/d\lambda$, as a rule, is less than zero, i.e., with an increase of strain, the rate of strain hardening decreases in absolute value. For convenience, the dependence $\eta - \lambda$ will be depicted with the opposite, i.e. with a positive sign on the graphs.

3. Study of hardening of cast austenitic steel 60X24AG16

3.1. Uniaxial extension

Fig. 2 shows the extension diagram of cast alloy 60X24AG16 at the speed of movement of the traverse of Instron 5582 $v = 0.3$ mm/min. The result of the digital recording of the experiment is shown by a solid line. The result of polynomial averaging of this diagram (dashed curve) is superimposed on the digital record of the diagram (continuous curve). It can be seen that there is a good practical agreement between the qualitative and quantitative characteristics of the averaged and experimental diagrams.

The ultimate tensile strength of cast steel is $\sigma_b = 987$ MPa for a given sample size, which is significantly higher than the ultimate tensile strength of structural steel 45 (640 MPa, rolled steel) [11]. This steel under uniaxial tension undergoes plastic strain $\varepsilon_p = 4.5 \pm 0.8\%$, which is $\approx 75\%$ of the total strain of the sample [7].

Figure 3 shows the dependences on the degree of stress strain σ, θ and η obtained as a result of processing the experimental material strain diagram using the above algorithm. The value Pa/% is the unit of measurement for θ accordance with the figure, and the value Pa/(%)^2 is unit of measurement for η. The unit of strain measurement in this case is the relative value $\Delta\lambda = \varepsilon = \Delta l/l_0$, where $l_0 = 48$ mm — length of the working part of the sample and Δl — increment of the length of the sample during strain. The strain diagram contained 593 points. Figure 4 shows for comparison similar dependencies obtained by the method proposed in Ref. [8], where the ratio $\Delta P/\Delta\lambda$ at any point of the diagram was determined by the difference in values ε through 25 points. It can be seen that the spread of points on the curves $\theta - \varepsilon$ and $\eta - \varepsilon$ remains significant despite the large interval between the points on the curve $\sigma - \varepsilon$.

The analytical averaging of the strain diagram (Fig. 3) completely eliminates the scatter of points. The strain interval within which the characteristics $\theta = \Delta\sigma/\Delta\varepsilon$ and $\eta = \Delta\theta/\Delta\varepsilon$ are located practically does not change. It is reduced by only 0.3% for η, however it decreases by 8.4% according to the method in Ref. [8].

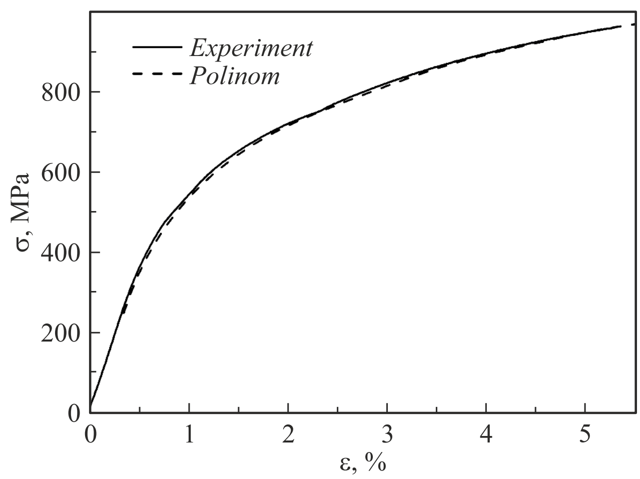

Figure 2. Extension diagram of cast steel 60X24AG16.

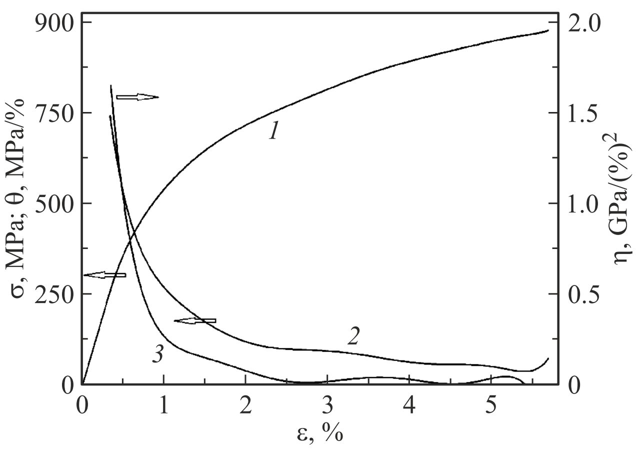

Figure 3. Dependence of stress σ (*1*), hardening θ (2) and hardening rate η (3) on strain ε.

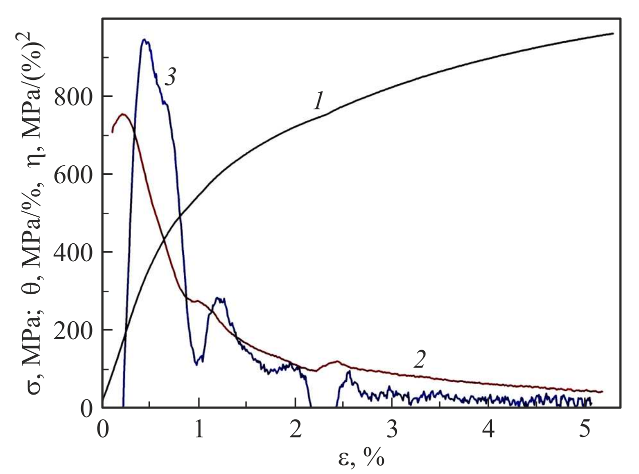

Figure 4. Dependence of stress σ (*1*), hardeningθ (*2*) and hardening rate η (*3*) on strain ε [8].

The coefficient of strain hardening is maximum and is equal to $\theta_{max} = 742$ MPa/% at the elastic strain stage. The onset of the plastic strain stage is recorded at a stress of $\sigma_0 = 251$ MPa, which is determined with high accuracy (not exceeding 0.01% of plastic strain). This value is 3 times less than the temporary tear resistance of the sample $\sigma_b = 976$ MPa and 2 times lower than the engineering yield strength $\sigma_{0.2} = 513$ MPa.

The decrease in the rate of strain hardening during strain occurs in two stages according to the dependence $\theta - \varepsilon$ (Fig. 3, curve *2*). First a sharp, then a smoother, decrease of θ from 742 to 100 MPa/% occurs at the initial stage (up to $\varepsilon = 2.5\%$). Then the rate of strain hardening slowly decreases from 100 to 35 MPa%, corresponding to the destruction point.

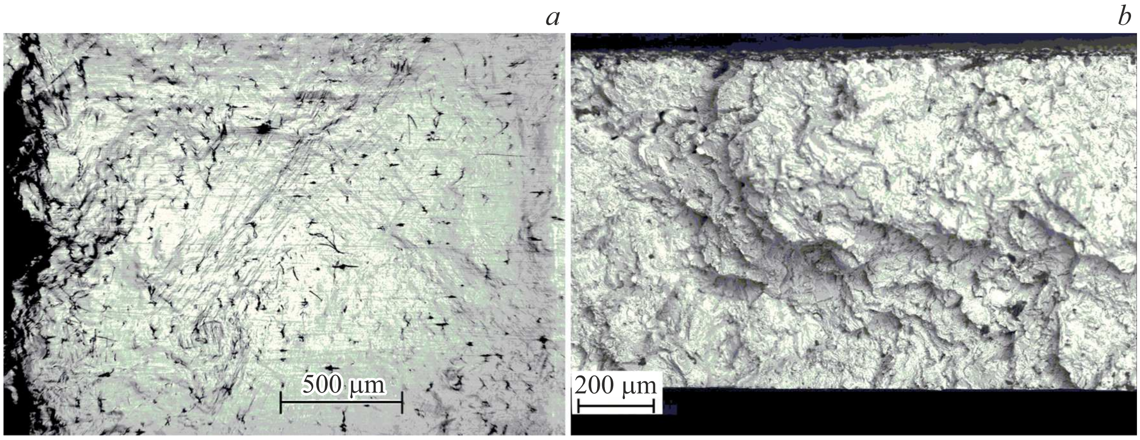

Figure 5. Metallographic picture of the front surface of the sample near the fracture area (*a*) and the fracture surface in the cross section of the sample (*b*).

The hardening rate $\eta = \Delta\theta/\Delta\varepsilon$ also changes in two stages (Fig. 3, curve *3*). η drops from the maximum value $\eta_{\max} = 1.65\,\text{GPa}/(\%)^2$ to zero at the first stage (up to $\varepsilon = 2.5\%$). Further, η remains almost within zero values until the destruction. This means that the decrease of θ occurs according to a linear law in this interval.

Figure 5 shows a metallographic picture of the relief of the front surface (Fig. 5, *a*) and the fracture surface in the section of the destroyed sample (Fig. 5, *b*).

The strain is distributed macro uniformly over the entire working length of the sample (Fig. 5, *a*).

Plastic strain can be judged only by thin slip marks oriented at an angle of 45° to the axis of tension. There are many microcracks on the front surface of the sample. There is no noticeable reduction of the sample cross-section in the fracture zone (Fig. 5, *b*). There are no signs of viscous fracture despite the presence of plastic strain. The picture of the surface relief in Fig. 5, *b* indicates the shear nature of the fracture.

3.2. 3-point deflection

It is of interest to determine the similarity and difference of the considered dependencies when changing the stretching mode to the 3-point deflection mode. The location of the sample on the supports is shown in Fig. 1. The peculiarity of the 3-point deflection tests is that the stress-strain state of the sample from the very beginning of loading is heterogeneous [8,12]. The layers of material adjacent to the point of application of force experience compression, and the layers on the opposite side experience stretching.

The measure of strain is the deflection value of the sample $\Delta\lambda = \Delta l$ in the case of a 3-point deflection. Experience has shown that there is a good agreement between the experimental and polynomial loading diagrams $P - \Delta l$.

The onset of the plastic strain stage is recorded at a load of $P_0 = 520\,\text{N}$, which is significantly less than the maximum load of the material $P_{\max} = 2.547\,\text{kN}$. The inelastic strain is $\approx 70\%$ relative to the total in this case. Thus, the elastic strain is quite significant at the moment of destruction. The strain hardening coefficient is maximum at the elastic strain stage and is equal to $\theta_{\max} \approx 3.0\,\text{kN/mm}$.

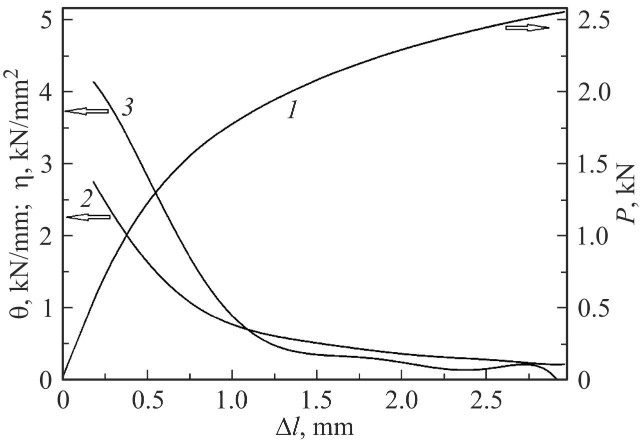

Figure 6. The dependence of the mechanical characteristics of cast steel 60X24AG16 on strain in the 3-point deflection mode. *1* — load P, *2* — hardening θ, *3* — hardening rate η.

Figure 6 shows the dependences of hardening θ and the hardening rate η on Δl. These curves have features that are similar to the case of uniaxial stretching (Fig. 3).

The onset of the plastic flow corresponds to the maximum value of the hardening rate $\eta_{\max} = 4.126\,\text{kN/mm}^2$.

The destruction of samples in the case of 3-point strain is also brittle. There are no traces of ductile fracturing (Fig. 7).

3.3. 3-point deflection, cyclic loading

Additional information about the mechanisms of strain hardening of cast steel 60X24AG16 is provided by an experiment on cyclic loading of a sample in the 3-point deflection mode. Figure 8 shows an experimental

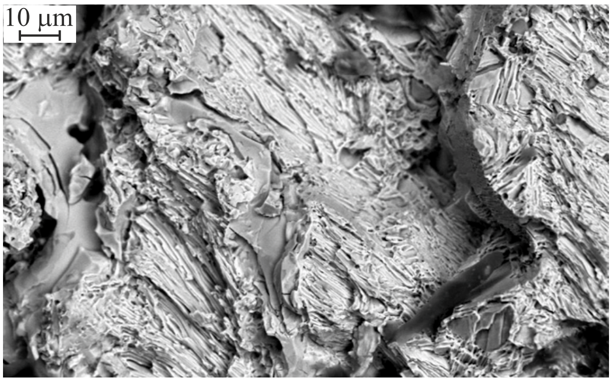

Figure 7. The fracture surface of the sample tested by 3-point deflection (SEM).

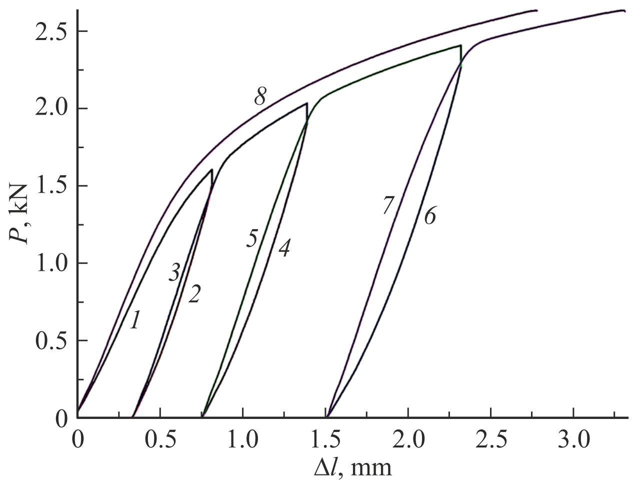

Figure 8. Experimental diagrams of cyclic loading. *1, 3, 5, 7, 8* — loading; *2, 4, 6* — unloading.

strain diagram of a sample that has undergone cyclic loading. Loading and unloading was performed at the same speed $v = 0.3$ mm/min. The sample was first loaded to $P_1 = 1600$ N (curve *1*), then completely unloaded (curve *2*) after a short pause (10−12 s). Next, the load and unloading curves of this sample were obtained in a similar way, which was loaded to $P_2 = 2027.0$ N (curves *3* and *4*), then to $P_3 = 2401.27$ N (curves *5* and *6*). The sample failed under load $P_f = 2524.94$ N (curve *7*) at the next loading. Figure 8 also shows the curve *8* for a sample tested without prior strain to failure at $P_f = 2623.53$ N.

The characteristic appearance of the unloading curves *2*, *4* and *6* is explained by the following reasons. The load drops during „load-unloading" switching for 10−12 s, when the sample is in creep mode. Consequently, the plastic strain of the sample continues. Apparently, it continues at the initial stage of unloading of the sample. On the other hand, Figure 8 shows that plastic strain partially returns during unloading in other local volumes of the sample. Obviously, there is a point on the unloading trajectory corresponding to the moment when the contribution of inelastic strain in the forward direction is balanced by inelastic strain in the opposite direction. The slope of the tangent is parallel to the elastic loading line at this point. The partial return of the inelastic strain of the sample increases as the force P_s increases at the start of unloading.

3.4. Effect of pre-straining

Figure 9 shows diagrams *1−3* without elastic strain stage after preloading to 1600, 2027 and 2401 N, respectively, starting from the start of plastic strain P_s. The diagram *4* is also presented for comparison, which was brought to destruction without prior strain. It can be seen that pre-strain significantly increases the moment of the start of the plastic strain stage P_s. A significant increase is observed immediately after the first loading to 1600 N (curve *1*). Repeated loading no longer results in a significant increase of the value of P_s (curves *2* and *3*). This is consistent with the results of studies in Ref. [13–16], where it is noted that a noticeable hardening of TRIP steel is observed even with 2% preliminary strain.

Fig. 10 clearly illustrates the dependence of the start of plastic strain P_0 on the preloading $P_{\max}$. Four experimental points allow representing the functional dependence $P_0 \approx f(P_{\max})$ in the form of a polynomial of the 3rd degree. Significant hardening from ≈ 500 to ≈ 950 N occurred immediately after the first loading to $P_{\max} = 1600$ N, when the plastic strain was no more than 7% of the total plastic strain of the sample.

The plastic strain partially returns in the unloading process, as shown in Fig.8. The inelastic return is equal to $\Delta l_b = 0.146$ mm after the sample loading to $P_3 = 2401$ N, which is 7.8% of the total plastic strain of the sample.

Figure 11 shows the dependences of two characteristics of the unloading curves on the preloading, namely the onset P_b and the magnitude Δl_b of the return of plastic strain.

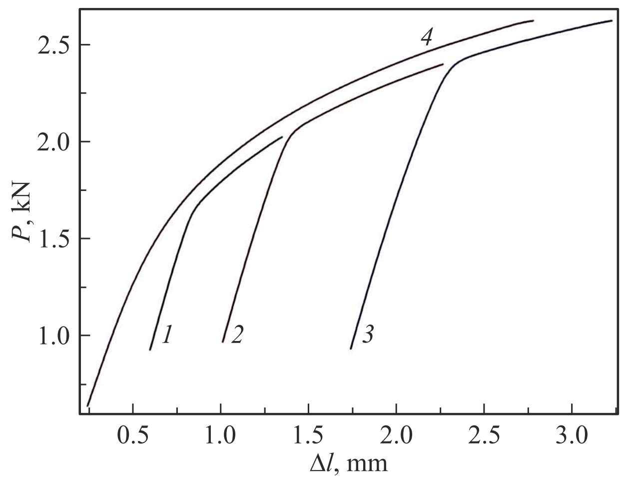

Figure 9. Strain diagrams without elastic stage in polynomial representation: *1−3* — after pre-straining; *4* — without pre-straining.

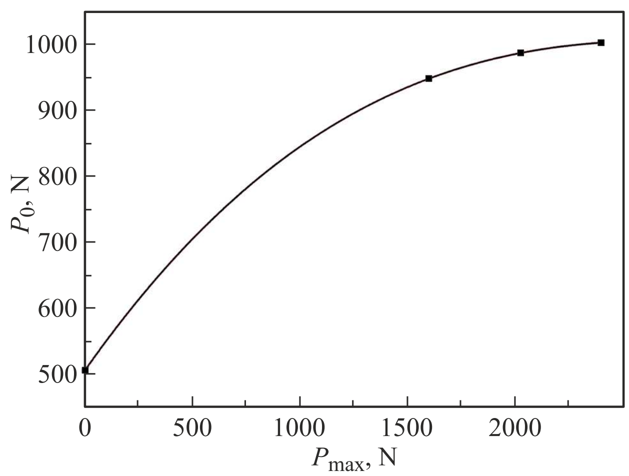

Figure 10. Dependence of the onset of plastic strain P_0 on the preloading P_{max}.

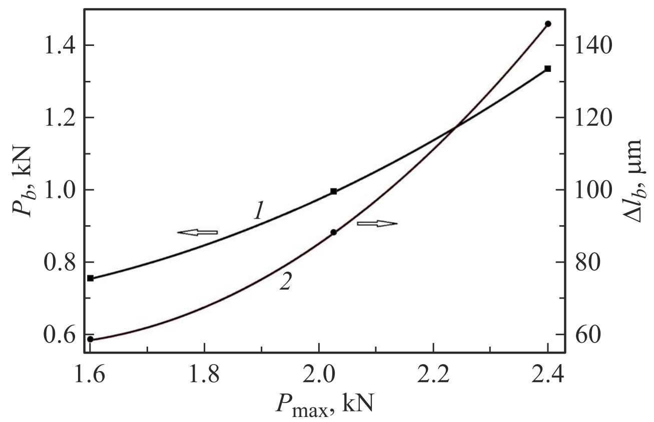

Figure 11. Dependences of the onset P_s (*1*) and the magnitude Δl_b (*2*) of the return of plastic strain on the preloading of the sample P_{max}.

These values increase significantly as the preloading increases, not according to a linear law. All three experimental points fit well on the curve of the polynomial dependence of the second degree.

Figure 12 shows the dependence of the coefficient of strain hardening on deflection Δl for a preloaded sample (curves *1–3*) and a sample without prestraining (curve *4*). It can be seen that the initial stage of dependence $\theta - \Delta l$ qualitatively changes after the preliminary straining. Two stages appear instead of a gradual decrease of the hardening rate. A smooth decrease of the hardening rate at the initial stage quickly passes into the second stage with a high hardening rate. However, very soon the dependence $\theta - \Delta l$ returns to the level characteristic of the sample without preloading.

Despite the low ductility, cast alloy 69X24AG16, due to its high strength, is characterized by good crack resistance. The stress intensity coefficient for this alloy is $K_{Ic} \approx 30\,\mathrm{MPa{\cdot}m^{1/2}}$ according to [17].

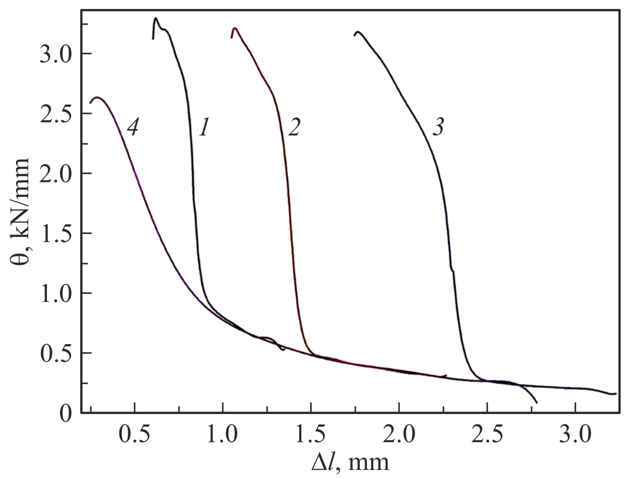

Figure 12. Dependences of the hardening rate on the strain of the sample: *1–3* — after preloading to 1600, 2027 and 2401 N, respectively; *4* — without prestraining.

4. Discussion

A method was used for the first time in this paper that allows to determine with great accuracy the characteristics of strain hardening of low-plastic metals and alloys, such as the speed and acceleration of strain hardening. The onset of the inelastic strain stage is determined with an accuracy of 0.008%.

The patterns of strain hardening of cast alloy 60X24AG16 are studied using this method.

It is shown that the alloy has high strength and fracture resistance with low plasticity not exceeding 5%. The temporary rupture resistance reaches the value $\sigma_b = 987\,\mathrm{MPa}$, and the stress intensity coefficient is $K_{Ic} \approx 30\ \mathrm{MPa{\cdot}m^{1/2}}$.

The dependences of the velocity θ and acceleration η of strain hardening have two stages regardless of the loading mode (stretching, three-point deflection). There is a quick and smooth transition from high values to low values in the first stage. Then comes the second stage when the decrease of these characteristics is slow. A similar behavior of the coefficient of strain hardening is observed in TRIP steels [10,18].

A characteristic feature of this alloy is the macrohomogeneous development of plastic strain, which prevents the formation of the neck. There is no noticeable reduction of the cross section of the sample in the fracture zone. There are no visible signs of ductile fracturing at magnification (Fig. 7, SEM) on the fracture surface despite the presence of plastic strain. The surface relief pattern indicates the shear nature of the fracture. The uniform nucleation of microcracks occurs during the straining process.

High strain hardening of alloys with residual austenite (TRIP steels) is associated with the phase transformation of γ-phases with a FCC lattice to phases ε and α' with HCP and BCC crystalline structures, respectively [11]. Martensitic $\gamma \rightarrow \alpha'$ transformation caused by local stress results in a decrease of stress concentration, an increase of the rate of strain hardening and uniform strain, followed by an increase of strength, toughness and plasticity [13]. Plastic strain propagates like a Luders band in low-carbon steels [1,6,19]. The transition of the soft phase of austenite to the hard and strong phase of martensite significantly prevents the development of plastic shifts throughout the sample volume. The material acquires the ability to undergo strong strain hardening. The processes of strong strain hardening mainly determine the initial stage of the characteristics of θ and η. The data obtained allow making an assumption about the presence of flat clusters of dislocations in front of obstacles in the form of martensite interlayers at grain boundaries [10,11].

The transition to the stage of a weak change in the rate of strain hardening is usually associated with the complexity of the nucleation of α'-martensite and the ease of transverse sliding of dislocations at higher external loads [10,11]. New slip systems are activated with an increase of the external load and extensive formation of packaging defects in austenite takes place. Paper [11] shows that the process of sequential formation of packaging defects is accompanied by the formation of ε-martensite.

According to [10], the strain associated only with the restructuring of the lattice during phase transformation $\gamma \to \alpha'$ for steel containing 5−15% of residual austenite is only 0.75−2.25%. It can be assumed that there is little residual austenite in cast steel 60X24AG16. Therefore, plastic strain should also be small attributable only to the phase transformation of metastable austenite into martensite [6]. However, it is this mechanism that promotes strong local hardening and prevents early localization of strain. The mechanical properties of cast steel are mainly determined by the mechanism of strain hardening due to martensitic transformation, rather than dislocation slip [8]. Papers [11] show that high values of the strain hardening rate are associated at this stage with the formation of ε-martensite and α'-martensite at the boundaries of ferritic grains, where clusters of dislocations are blocked by Lomer-Cottrell atmospheres.

Additional information is provided by experiments on cyclic loading of a square-section rod using the 3-point deflection method. It was found that a partial return of inelastic strain occurs during unloading. Preliminary plastic strain by only 0.3% results in a strong strain hardening of the material.

The return of plastic strain during unloading may be attributable to the fact that there is a reverse movement of dislocations in clusters in front of obstacles [20]. In addition, the contribution from partial or complete collapse of microcracks caused by pre-straining cannot be excluded.

Conclusions

The conducted studies have shown that cast alloy 60X24AG16 is a full-fledged structural material with high rates of strain hardening, strength and fracture resistance.

The results obtained on the example of cast alloy 60X24AG16 can be used in experiments, as well as in theoretical models and numerical calculations of the mechanical properties of low-plastic materials for more accurate prediction of the behavior of austenitic stainless TRIP steels.

Funding

The research has been performed under the state assignment of the Institute of Strength Physics and Materials Science of the Siberian Branch of the Russian Academy of Sciences (project No.FWRW-2021-0009.

Conflict of interest

The authors declare that they have no conflict of interest

References

[1] M. Kucharska, S. Wiewiórowska, J. Michalczyk. A. Gontarz. Materials, **13** (5769), 1 (2020). DOI: 10.3390/ma13245769

[2] R.R. Magalhãesa, F.S. Costab, B.M. Gonzalezc. Mater. Res., **22** (4), e20190088 (2019). DOI: 10.1590/1980-5373-MR-2019-0088

[3] B.C. De Cooman. Current Opinion in Solid State and Mater. Sci., **8**, 285 (2004). DOI: 10.1016/j.cossms.2004.10.002

[4] A. Petrov. High-strength TRIP or PNP steels. https://heattreatment.ru/vysokoprochnye-trip-trip-ili-pnp-stali.html

[5] N. Lun, D.C. Saha, A. Macwan, H. Pan, L. Wang, F. Goodwin, N. Zhou. Mater. Design, **131**, 450 (2017). DOI: 10.1016/j.matdes.2017.06.037

[6] F.G. Caballero, H.K.D.H. Bhadeshia, K.J.A. Mawella, D.G. Jones, P. Brown. Mater. Sci. Technol., **18** (3), 279 (2002). DOI: 10.1179/026708301225000725.

[7] E.E. Deryugin, N.A. Narkevich, Yu.F. Gomorova. Izvestiya. Ferrous Metallurgy, **65** (12), 879 (2022). DOI: 10.17073/0368-0797-2022-12-879-886

[8] E.E. Deryugin, I.V. Vlasov, Yu.F. Gomorova. Russ. Phys. J., **66** (12), 1242 (2024). DOI: 10.1007/s11182-023-03068-y

[9] N. Saenarjhana, J.-H. Kanga, S. Ch. Leeb, S.-J. Kim. Mater. Sci. Eng. A, **679**, 531 (2017). DOI: 10.1016/j.msea.2016.10.062

[10] P. Spätig, R. Schäublin, M. Victoria. Mat. Res. Soc. Symp. Proc., 683E, 1 (2001). DOI: 10.1557/PROC-679-BB1.10

[11] GOST 11050-88. *Interstate standard. Long-rolled products, calibrated, with special surface finishing, made of high-quality carbon structural steel* (M.: IPK Standards Publishing House, 2003)

[12] M.N. Grebennikov, N.I. Pekelny. *Geometricheskie harakteristiki ploskih sechenij uchebnoe posobie* (Nats. aerokosm. un-t im. N.E. Zhukovskogo „Khark. aviats. in-t“, Kharkov, 2015), s. 92. (in Russian).

[13] A. Barcellona, L. Cannizzaro, D. Palmeri. Key Engineer. Mater., **344**, 71 (2007).

[14] G. Sanyal. Modern Approaches on Mater. Sci., **5** (3), 705 (2023). DOI: 10.32474/MAMS.2023.05.000211

[15] E. Billur, S. Karabulut, I. Yílmaz. Hittite J. Sci. Eng., **5** (3), 231 (2018). DOI: 10.17350/HJSE19030000100

[16] K. Davut. *Relation between Microstructure and Mechanical Properties of a Low-alloyed TRIP steel* (Shaker Verlag, Aachen, 2013), p. 129.
[17] E.E. Deryugin, A.V. Pazhin. Russ. Phys. J., **66** (12), 1270 (2024). DOI: 10.1007/s11182-023-03072-2
[18] P. Behjati, A. Najafizadeh, A. Kermanpur. Mater. Sci. Technol., **27** (12), 1828 (2011). DOI: 10.1179/1743284710Y.0000000040
[19] H.K.D.H. Bhadeshia. *Bainite in steels. Theory and practice. Third edition* (University of Cambridge and Postech, 2015), p. 589. DOI: 10.1201/9781315096674
[20] J. Hirt, I. Lote. *Teoriya dislokatsi* (Atomizdat, M., 1972), s. 600. [Transl. from English. Edited by E.M. Nadgorny, Yu.A. Osipyan]

Translated by A.Akhtyamov